Facies — The drivers for modern inversions

John Pendrel[1] and Henk Schouten[1]

https://doi.org/10.1190/tle39020102.1

Abstract

It is common practice to make facies estimations from the outcomes of seismic inversions and their derivatives. Bayesian analysis methods are a popular approach to this. Facies are important indicators of hydrocarbon deposition and geologic processes. They are critical to geoscientists and engineers. The application of Bayes' rule maps prior probabilities to posterior probabilities when given new evidence from observations. Per-facies elastic probability density functions (ePDFs) are constructed from elastic-log and rock-physics model crossplots, over which inversion results are superimposed. The ePDFs are templates for Bayesian analysis. In the context of reservoir characterization, the new information comes from seismic inversions. The results are volumes of the probabilities of occurrences of each of the facies at all points in 3D space. The concepts of Bayesian inference have been applied to the task of building low-frequency models for seismic inversions without well-log interpolation. Both a constant structurally compliant elastic trend approach and a facies-driven method, where models are constructed from per-facies trends and initial facies estimates, have been tested. The workflows make use of complete 3D prior information and measure and account for biases and uncertainties in the inversions and prior information. Proper accounting for these types of effects ensures that rock-physics models and inversion data prepared for reservoir property analysis are consistent. The effectiveness of these workflows has been demonstrated by using a Gulf of Mexico data set. We have shown how facies estimates can be effectively used to build reasonable low-frequency models for inversion, which obviate the need for well-log interpolation and provide full 3D variability. The results are more accurate probability-based net-pay estimates that correspond better to geology. We evaluate the workflows by using several measures including precision, confidence, and probabilistic net pay.

Introduction

In recent years, facies analysis from the outcomes of seismic inversions has become an integral part of reservoir characterization. Our use of the term "facies" refers to geophysical or geologic layers to which petrophysical, geophysical, or geomechanical measurements can be associated. In this context, terms such as "lithofacies" or "lithotypes" may be more appropriate. Nevertheless, we prefer to use the more popular term "facies" here. Facies are an excellent starting point for meaningful conversations between geophysicists and geologists and are critical to engineering decisions. They can also have reservoir simulation applications in defining the heterogeneity of reservoirs between wells. In this context, we can write the Bayesian probability as posterior = likelihood × prior/normalization, or:

$$p(c_i \mid x) = p(x \mid c_i)\, p(c_i) \Big/ \sum_{i=1}^{N} p(x \mid c_i) p(c_i) \,, \qquad (1)$$

where $p(x|c_i)$ is the likelihood ratio, $p(c_i)$ is the prior probability, and $p(c_i|x)$ is the posterior probability (Hossain et al., 2015).

Mur and Waters (2018) demonstrate an inversion that utilizes a Bayesian framework to iteratively construct a facies and impedance model using prior estimates of facies distribution and impedance uncertainty. See Kemper and Gunning (2014) and Sams et al. (2016) for further examples. Gonzalez et al. (2016) use rock-physics models to complete the facies definition set for those facies not encountered by wells. They also compute spatially variant priors, which are consistent with geology, to determine the 3D distribution of Bayesian facies probabilities. Merletti and Torres-Verdin (2006) use a simultaneous joint geostatistical inversion for elastic properties and lithotypes to enforce per-facies rock-property relationships and image thin bedding in a clastic setting. See Saussus and Sams (2012), Hameed et al. (2016), Singh et al. (2016), and Tao et al. (2016) for similar applications. Initiatives to integrate facies and inversions with machine learning are becoming more common (Yenwongfai et al., 2019). Machine learning has also been used to generate petrophysical facies curves (Hall, 2016; Hall and Hall, 2017; Guarido, 2019; Nishitsuji and Exley, 2019). Machine learning is applied to ensure that all disparate information is used most effectively toward a solution. In this context, it is not very different from what occurs in the Bayesian world, where we ensure that priors represent and contain all previously available information. It is this direction that we have followed here.

Facies inversion workflows

Bayesian inference. In our investigations of the applications of facies to reservoir characterization, we have taken a Bayesian approach. Bayes' rule is uniquely positioned as a reservoir-characterization tool because of its amalgamation of prior information and new measurements. The results are probability based, which lead naturally into determinations of risk. Here, we use Bayesian inference to determine the probabilities of occurrence of geologic facies from seismic reflection data and in particular, from AVO inversions (Pendrel et al., 2006). It is observed that facies, when displayed in a crossplot space defined by inversion outcomes, commonly exhibit a clustering behavior. This clustering can be described by assigning joint probability density functions (PDFs) to each facies. Applying Bayes' rule provides the probability of occurrence of each of the facies at every location in 3D space. Volumes of the most-probable facies follow. The design of the PDFs comes initially from well-log data but can be augmented

[1]CGG, Calgary, Alberta, Canada. E-mail: john.pendrel@cgg.com; henk.schouten@cgg.com.

by rock-physics modeling or any other available information. The properties in crossplot space can be any derivative of seismic inversions. For example, quartz volume and brittleness have been used in an unconventional shale play (Varga et al., 2012).

Low-frequency models. When the process is complete and we have determined facies from the inversion elastic data everywhere in space and time (or depth, in the case of depth inversions), the output facies probabilities can be used for a purpose beyond mapping the most probable facies. Coupled with per-facies elastic trends measured from logs or computed from rock physics, low-frequency models with full 3D variability can be constructed (Pendrel et al., 2016). In its simplest form, the trend value corresponding to the most probable facies is chosen and assigned. We have used a weighted approach, where all facies contribute, their probabilities of occurrence acting as the weights. This new low-frequency model can be used in a second pass of inversion and subsequent facies analysis.

Probability threshold. The facies probability volumes are also useful in computing reservoir attributes such as net pay. We implement a probability threshold, below which data samples do not count toward net-pay calculations. We need to be able to discriminate between reliable and less-reliable facies estimations, where the limited resolving power of the input parameters and their measured uncertainties combine to reduce facies probabilities. This allows us to bring the required level of confidence to net pay and other similar derivatives.

Petrophysical facies. We also applied the Bayesian process to the problem of identifying time-domain petrophysical facies from wireline logs (Pendrel et al., 2017). These facies can be mapped from the petrophysical to elastic domain for use by geophysicists and engineers. Prior information can be declared to be uniform (all facies probabilities equal) or implemented by log probability (proportion) curves representing core observations or any other prior facies estimates. The challenge is to preserve some petrophysical meaning in the elastic facies, which will ultimately be of real use to interpreters and modelers. The elastic properties are intended to be proxies for petrophysical properties and allow us to estimate petrophysical facies from elastic data. We need to ensure, as a quality-control step, that this assumption is correct within the seismic band. This could require redefinition or regrouping of the petrophysical facies or the selection of alternate elastic properties.

Of critical importance is the development of priors for the Bayesian estimation of elastic facies. It is common to use the uniform or some proportional percentages based on the relative occurrences of the facies in well logs. However, this approach ignores any geologic ordering of facies, which should be considered as a part of prior information (Pendrel et al., 2017). The choice of prior probabilities can be critical. It is important to fairly represent the state of our present knowledge before the addition of further evidence from seismic inversions. We construct initial priors with probabilities from the petrophysical facies analysis described earlier, averaging over wells and ensuring structural compliance. Except for structure, this ignores well-to-well lateral variations in facies thickness. However, our purpose will be to use this construct as a 3D prior for the probabilities of finding the various facies in our subsequent analyses. In this context, it is superior to using simple facies proportions or the uniform distribution. The results are 3D prior volumes, which are laterally constant but structurally compliant. As in the case of the estimation of petrophysical facies, prior uncertainties can be implemented so that the priors act as guidelines rather than *de facto* decisions. Prior information can also be included in the form of rock-physics templates, which are commonly overlain on the PDFs in facies design templates. They provide a useful guide when well-log information is limited or does not include all of the facies and fluid possibilities.

Uncertainties. Although the results of deterministic inversions produce single values, there is associated uncertainty in these inversions, whether we acknowledge it or not. Inversion uncertainties in the seismic band can arise from a host of possible causes, including random and coherent noise and multiple interference, wavelet uncertainty, etc. See Thore (2015) for more detailed discussion. Apart from uncertainties, there is always the possibility of inversion bias. Biases can be variable from one geologic layer to the next and result from our attempts to image very thin layers. They can also be caused by attempts to account for lateral variabilities in facies property trends by the interpretation of well logs and the extension of the low-frequency model (LFM) band with ultra-low-frequency stacking velocity information. The use of inaccurate or inappropriate per-facies trends in LFM design can also contribute to inversion bias.

A rigorous approach to uncertainty estimation may involve estimating the uncertainties in each of the inversion inputs and from these, the net uncertainty in the inversion outcomes. Here, we take a more phenomenological approach. We estimate uncertainties by crossplotting inversion outcomes at well locations versus high-cut filtered logs (Pendrel et al., 2016). The residuals referenced to best-fit regressions are plotted as a histogram and modeled with uncertainty probability density functions (uPDFs). The uPDFs are quite often Gaussian or log Gaussian, but need not be. Since the elastic probability density functions (ePDFs) are actual density functions, a probability estimate corresponding to a field measurement should not be obtained by simply reading a PDF value. Rather, it should involve integration under the PDF curve. The uPDFs provide the template for doing this. The use of uPDFs has another benefit. Certain bias conditions existing in the inversions will result in the means of the uPDFs becoming nonzero. However, once that information becomes encoded in the uPDFs, bias is automatically corrected during the Bayesian process.

Quality control. Quality control of facies estimations can be accomplished in several ways. We favor a close-the-loop approach, wherein the facies templates applied to inversion data are also applied to the corresponding filtered well logs and the results are compared. This applies not only to facies estimated from the native results of inversions (typically P-impedance, V_P/V_S, density, etc.), but also any derivatives such as shale volume or porosity. We have recently found a confidence measure based on the Shannon (1948) definition of entropy to be useful (Pendrel and Schouten, 2019). It is clear that regions where the probabilities of the two most probable facies are almost the same are less reliable than if a single facies had been the clear winner. A confidence index (CI) with range from zero to unity is derived from negative-scaled entropy. The latter is computed from:

$$H = -\sum_{i=1}^{N} p_i \ln(p_i) \ , \qquad (2)$$

where p_i is the probability of the i^{th} facies in the set of N.

The CI is a useful measure to compare facies determined from different inversion strategies and is also relevant in measuring the consistency of sets of realizations from geostatistical inversion. It also comes into play when attempting to understand the number of facies, which can be supported by petrophysics and ultimately, in the elastic domain, by seismic inversions. Should attempts be made to define too many facies, given the wireline logs and band-limited inversions at hand, the CI will not approach acceptable levels (typically approximately 0.8 in the authors' experiences). When inversion uncertainties, modeled or real, are included, their effects on the CI can also be determined. The number of available wells does not directly affect the CI since it is a function of only the probabilities from the Bayesian analysis. There can be an indirect connection since the facies priors can be constructed from observations at the wells. More wells can lead to greater confidence in the priors and the assignment of smaller uncertainties. To date, we have implemented uncertainty priors on a geologic layer-by-layer basis only. Spatial variation is a possibility that we have considered in future work.

Gulf of Mexico example

We test the previously stated ideas with a Gulf of Mexico data set. The key horizon is the top of the Green sand shown in Figure 1. Below the Green horizon, we recognize upper and lower Green sandstones, since the facies statistics are slightly different. Sharp discontinuities in the figure are indications of faulting. Geologically, there is a set of two vertically stacked deltaic systems of Middle Pliocene age. They average approximately 400 ft in thickness and are separated by approximately 500 ft. Within the play area are delta slope deformation, slump-induced turbidites, and thin mouth-bed deposits, without the presence of delta plain facies. The principle facies are shale, silt, and pay sand.

Three logs in five wells were used to define the facies: water saturation (S_w), shale volume (V_{sh}), and density porosity minus neutron porosity (ΦND). Figure 2 shows the PDF design templates used to build the facies curves. The prior probabilities were taken to be the uniform distribution, as no other information was available. The resulting facies curves are also shown in Figure 2. Figure 2 admits the possibility of inputting core information as a prior or for calibration. We did neither in this work. The output facies probabilities at each well location can be used for one further purpose. Coupled with per-facies elastic trends measured from logs or computed from rock physics, they can be used to create a new low-frequency model

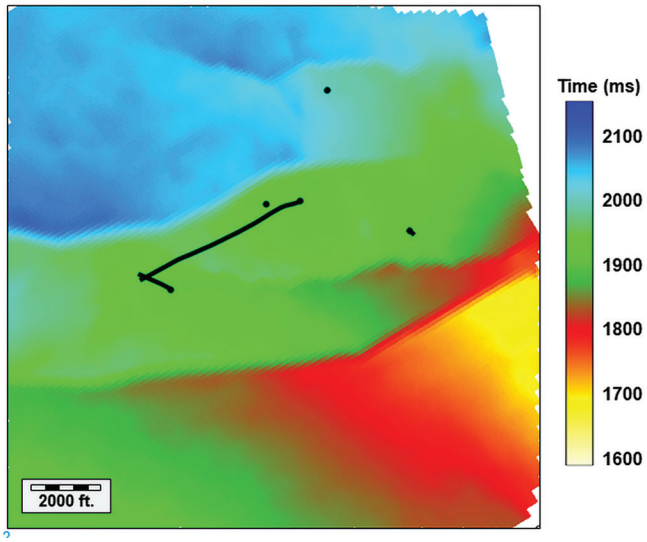

Figure 1. Project map showing the Green horizon and five well locations.

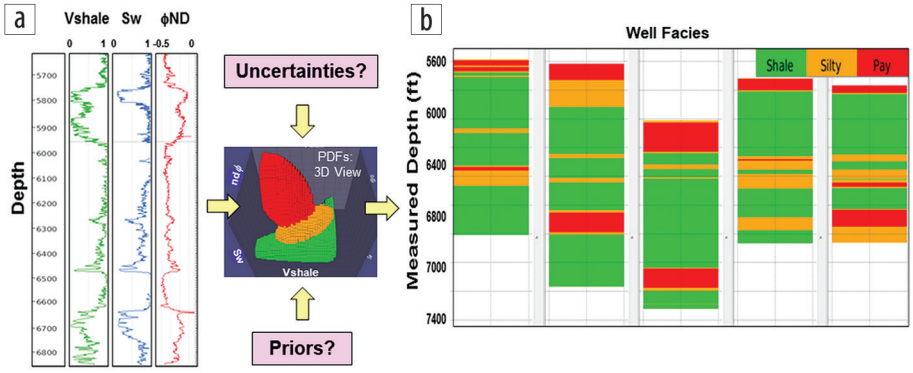

Figure 2. PDF template for (a) Bayesian petrophysical facies analysis and (b) output petrophysical facies at key wells. The process admits the possibility of uncertainties and priors, although none were used. All five wells contributed to the analysis.

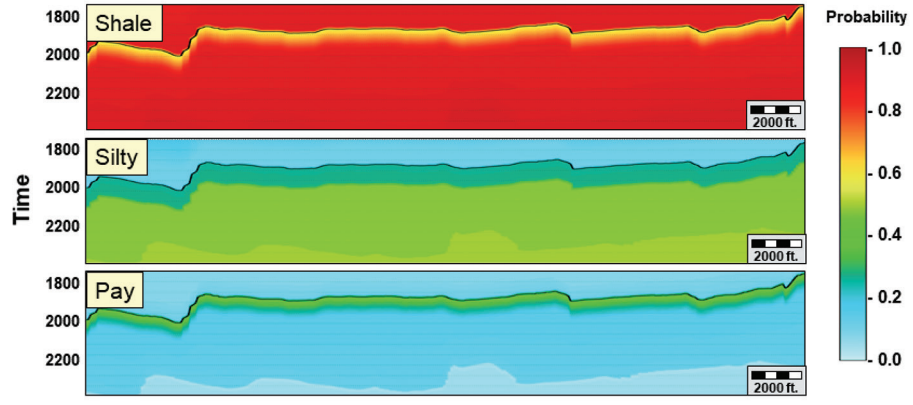

Figure 3. Probability trends derived from the original Bayesian petrophysical facies analysis of the well data. Well averages of facies probabilities from the Bayesian analyses in Figure 2 were determined and made to be structurally compliant.

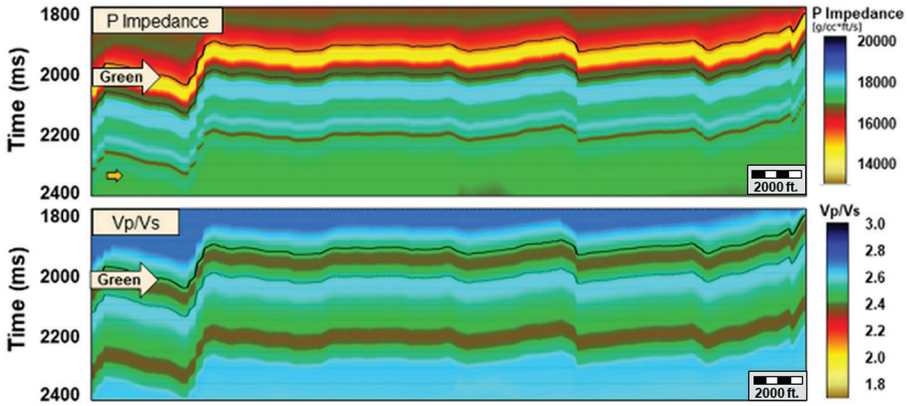

Figure 4. Constant but structurally compliant elastic property trends constructed from averages over all of the wells. These were used as low-frequency model input for the first inversion workflow.

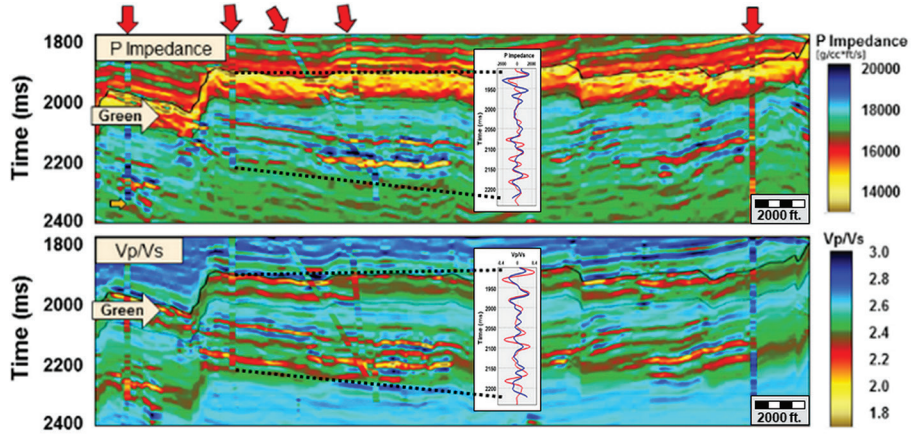

Figure 5. P-impedance and V_P/V_S from an absolute inversion with high-cut filtered logs at the well locations (arrows). Disagreements are caused mainly by the fact that only average trends were used. No well-log interpolation was done. The well on the right is in a different pressure regime and shows more disagreement with respect to average values. The tie at one well has been expanded to show greater detail within the seismic band. The blue curve is the well log, and the red curve is the inversion along the well path.

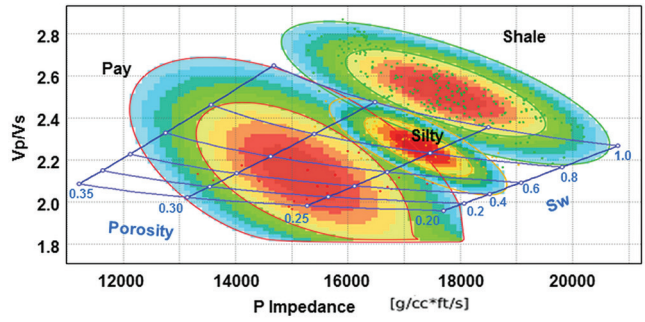

Figure 6. In this facies PDF design template, facies ePDFs are shown in elastic crossplot space along with high-cut filtered well-log data. A rock-physics template is also used as a design guide. The ePDF contours represent first and second standard deviations.

with complete 3D variability, which we constrain to be structurally compliant (Figure 3). These will make useful priors when we are ready to estimate facies from inversion.

The available seismic consisted of five partial-angle stacks. The maximum angle in the farthest stack was 50°. This was not judged to be sufficient to resolve density with any degree of certainty. A single set of wavelets, one for each partial stack, was obtained by matching elastic synthetics to the seismic at each of the five available wells, some of which were deviated. The log sets included full-wave sonic logs over the reservoir interval, facilitating the creation of the AVO wavelets. A simultaneous AVO inversion algorithm (Debeye and van Riel, 1990; Pendrel et al., 2000) was used to create the inversions.

Absolute inversions require a realistic low-frequency model. This is sometimes problematic when the reservoir properties manifest partially in the low-frequency band, below that of the seismic. This was the case in our example. The lower limit of the seismic band was estimated to be 12 Hz. In these cases, a simple trend will not do — the low-frequency model must be rich in frequencies up to the lower limit of the seismic band to characterize thinner pay-bearing layers. We constructed such a model by creating frequency-rich (in the band below the seismic) average elastic property curves from all of the wells and making them structurally compliant (Figure 4). We refer to this as the "constant trend workflow." The inversion results obtained after the application of this workflow are shown in Figure 5 along an arbitrary line passing through all the wells and with high-cut filtered well logs overlain. The matches are not perfect since the inversion has no prior knowledge of the high-frequency component of the logs and the low-frequency model was made from well-log averages. It would have been an easy procedure to build the low-frequency model with some sort of lateral well-log interpolation scheme to ensure better matches at the wells. However, this raises other issues related to the validity of any type of interpolation method. We have followed the popular custom to avoid this approach here, although it is part of our planned future work. The region of interest in Figure 5 is the Green sand (horizontal arrows), where there is the possibility of hydrocarbon deposits. The P-impedance agreement with the wells is good, and the V_P/V_S is fair.

The facies design template is shown in Figure 6. The ePDF contours represent the first and second standard deviations. Indications are that the pay facies will be well separated from others and should be well imaged. This is a result of the fact that the pay facies exhibit high porosities and are gas charged. Shale and silt are less well separated. A rock-physics template designed for this reservoir is overlain and leads us to replace the pay facies ePDF with the truncated version in the figure since no very low V_P/V_S facies are indicated by the rock-physics template or observed. We note that the number of well-log data points

representing any particular facies can be variable and sometimes quite small. While not a real problem for these data, it could become an issue in other situations. The standard deviation of the ePDFs should reflect any such lack of knowledge resulting from a lack of data. Rock-physics models as illustrated here can help ameliorate the situation. It is also possible that the inversion data represent a facies not encountered by any of the wells and heretofore unknown. We set a limit to the facies classifications, typically at three standard deviations. Any facies outside of this limit for every defined ePDF are labeled "unclassified." Analysis and mapping of these unclassified facies can often result in a better understanding of the geology and the addition of new members to the facies set. The results of the uncertainty analyses of the inverted P-impedance and V_P/V_S ratio are shown in Figure 7. The background histograms, to which the uncertainty PDF is modeled, are residuals from best-fit lines between high-cut filtered logs and inversion results at the well locations. These modeled uPDFs become inputs to the Bayesian inference process. Note the presence of small biases where the mean residual is not zero. These are now being accounted and corrected for in the Bayesian analysis. We modeled the uPDFs approximately with Gaussians although any function, including a rigorous fit to the histogram (binning), could have been used. The important thing is to include a reasonable amount of uncertainty in the Bayesian process. We were driven at all times to achieve the highest accuracy with respect to the known facies at the wells, adjusting the input parameters to do so. Somewhat counterintuitively, we find that the addition of uncertainty sometimes increases accuracy at a given probability threshold by changing facies assignments or decreasing their probabilities of occurrence. Potentially incorrect facies assignments are assigned increased uncertainty. The associated decrease in probability can result in the assignment not achieving an acceptable probability threshold for facies to count in net pay or similar calculations. Therefore, risking by the strategy of probability thresholding in the calculation of net pay can remove dubious facies assignments from the analysis.

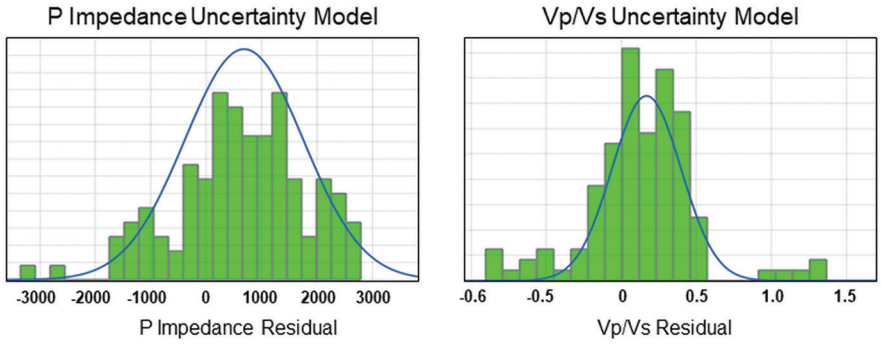

Figure 7. Gaussian fits to log inversion crossplot residuals are shown for P-impedance and V_P/V_S. The histograms are residuals between high-cut filtered logs and inversions at the well locations. The means and standard deviations of these uPDFs are included in the Bayesian inference process.

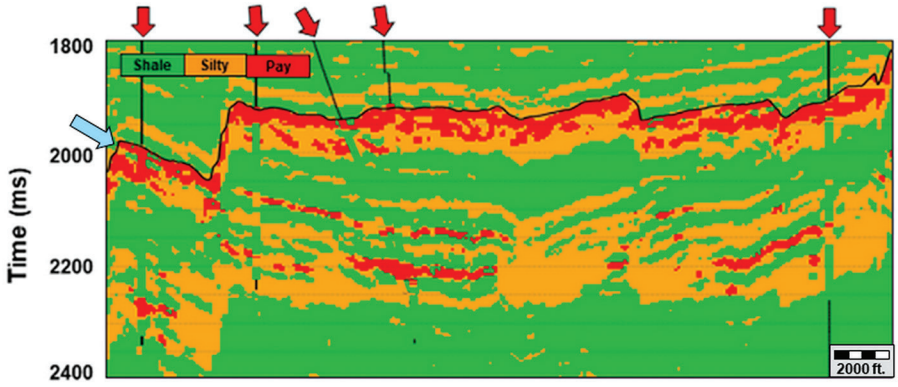

Figure 8. Facies from the inversion with the constant trend method. The same process was applied to the well-log curves, and those resulting facies are shown in overlay. A qualitative assessment shows basically good agreement at the well locations. The blue arrow indicates a poor tie, which we believe is multiple related.

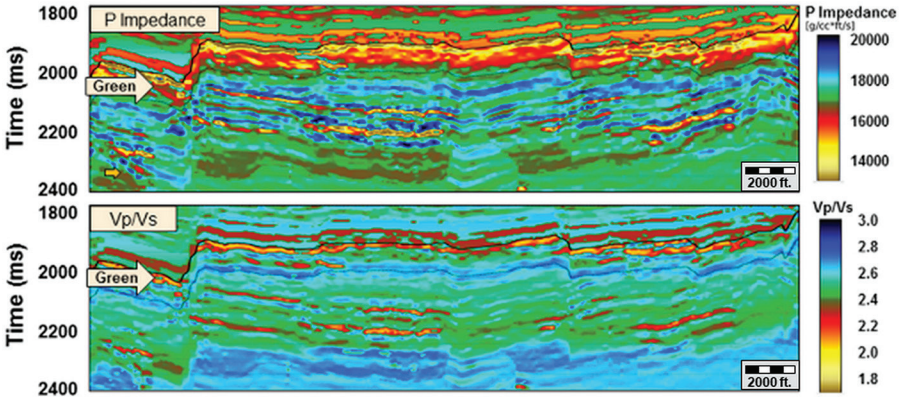

Figure 9. The facies in Figure 8 were combined with per-facies trend information derived from the wells to build a facies-driven model for use as a low-frequency model in an AVO inversion. This was done by assigning per-facies trend values corresponding to the estimated facies and applying the facies-weighting method described in the text. This model shows spatial variability not present in the constant model (Figure 4). Although the model created was broadband, only the low-frequency portion (less than or equal to 12 Hz) was used in the inversion.

In Figure 8, we show the most probable facies with the well facies overlain. There is generally decent agreement with the well facies, and the pay facies are well imaged. There is notable disagreement between the well and the inversion at the far left well just below the Green horizon, where shale instead of pay is indicated (blue arrow). This was determined to be a real effect from the inversion and could possibly indicate a multiple problem.

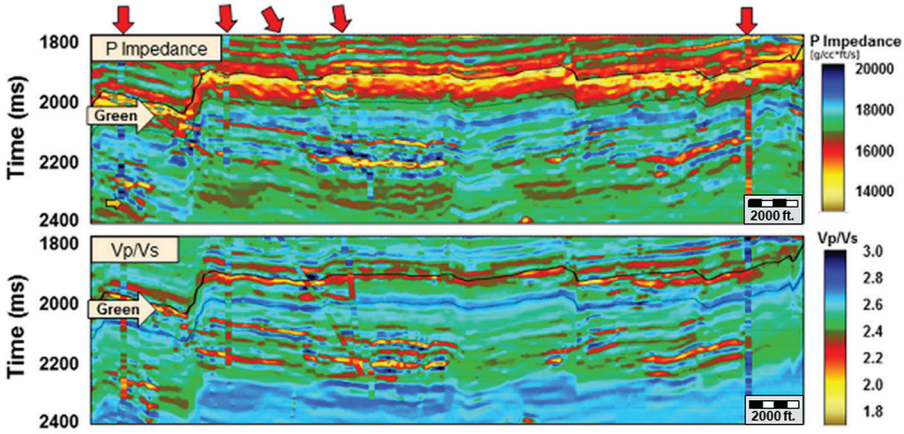

Figure 10. Results of an AVO inversion incorporating the low-frequency model constructed from the facies in Figure 8 and per-facies trends from logs.

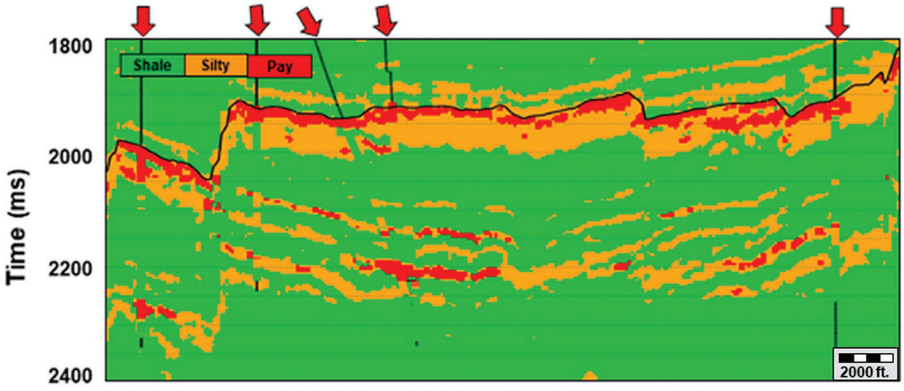

Figure 11. The inversion was rerun using a filtered version of Figure 9 for a low-frequency background model and the facies was reestimated. Again, the well-log facies have been overlaid.

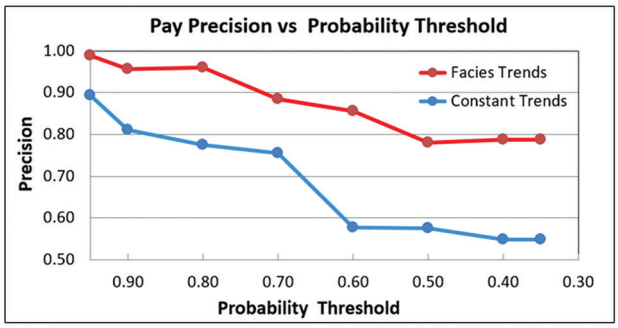

Figure 12. This precision analysis compares the facies from the constant (blue) and facies-driven (red) inversion workflows. These differed only in their input low-frequency model. For each, precision measures were computed in a standard way, except only winning probabilities above the threshold were considered. The facies-driven model is better overall due, in particular, to its spatial variability facilitated by the facies estimates. This is especially true for those thresholds that explorationists would consider to be viable. Thresholds of at least 0.80 are preferred by the authors.

Deeper in the section, there is perhaps too much silty facies. This is an anticipated point of confusion, given the juxtaposition of the shale and silty ePDFs (Figure 6). The overall result could be improved by upgrading the LFM input to the inversion. This can be done by combining the facies from the constant method with per-facies trends derived from well logs (or rock-physics models) to create new broadband property models (facies-driven workflow). In doing this, we split the shale category into three members to ensure that the data limits in P-impedance V_P/V_S space are well represented. At each time in the section, per-facies elastic trend values are assigned to the output model depending on the facies. We used the weighted approach discussed earlier to construct the output trend from a probability-weighted sum of the contributions from all facies members. These results are shown in Figure 9 and are used as low-frequency (less than or equal to 12 Hz) model inputs in another round of prestack AVO inversion. Small changes in the ePDFs, uPDFs, and prior uncertainties were made to improve precision. The 3D priors were the estimated facies probabilities from the constant method with prior uncertainties included. Prior probability uncertainties soften the effects of the priors and ensure that the result is not predetermined by them. In the case of the upper sandstone, they were set to 0.30, 0.20, and 0.50 for the shale, silty, and pay facies, respectively. The final results are significantly affected by the prior uncertainty settings, but are not overly sensitive to them. Mainly, they affect the probabilities of the assigned facies. We set them for optimal well matches at a probability threshold of 0.80. The second pass of inversion is shown in Figure 10. The resulting facies analysis from that inversion is shown in Figure 11. Note the reduced amount of pay in the upper part of the reservoir and the reduced presence of silty facies deeper.

With respect to the difference between the log and estimated facies, there is not much difference between Figures 8 and 11. However, a more detailed analysis highlights the differences. We used the definition of precision (Liu et al., 2019), which is the number of true positive classifications divided by the sum of the true positives and the false positives. We considered the precision for pay, modifying it with the notion of thresholding. We usually are not interested in pay classifications where the probabilities of occurrence are not high. Therefore, we eliminate them from the precision calculation. We computed a set of precision measures at all of the wells for a range of probability thresholds, only omitting the suspect area described earlier and highlighted in Figure 8. The results for both inversion workflows are shown in Figure 12. Clearly, the inversion incorporating the facies-driven low-frequency model outperforms the constant trend method everywhere and especially at any thresholds of real interest. This is because we use facies estimates to create a laterally varying low-frequency model, which is an improvement over a single

constant model with spatial variability arising solely from the requirement for structural compliance. Models made from some form of well-log interpolation would certainly perform better at the wells, but their validity could not be guaranteed between them. This has been the classic approach but is not considered here for these reasons.

We created upper sand net-pay maps from both workflows (Figure 13). In the upper panels, the probability threshold used was 0.8, and the data samples were further weighted by probability. The constant method shows greater net pay compared to the facies-driven workflow. We interpret this to be the manifestation of the greater number of false positives indicated in Figure 12. The lower panels compare the facies-driven workflow for thresholds of 0.7 and 0.9. There is naturally less pay with the higher threshold, but it comes with greater reliability. Perhaps, the 0.7 threshold map best shows evidence of clinoform development in the northeast.

In Figure 14, we compare the CI for the constant and facies-driven workflows. The CI in the facies-driven method is significantly higher overall. The constant method demonstrated less confidence in discriminating facies. However, the pay facies from the constant method were generally well imaged, suggesting that it is a viable procedure for a first look at the key facies. Both methods have issues separating some shale and silty facies. This was anticipated from the ePDFs in Figure 6 and exacerbated by the uPDFs in Figure 7.

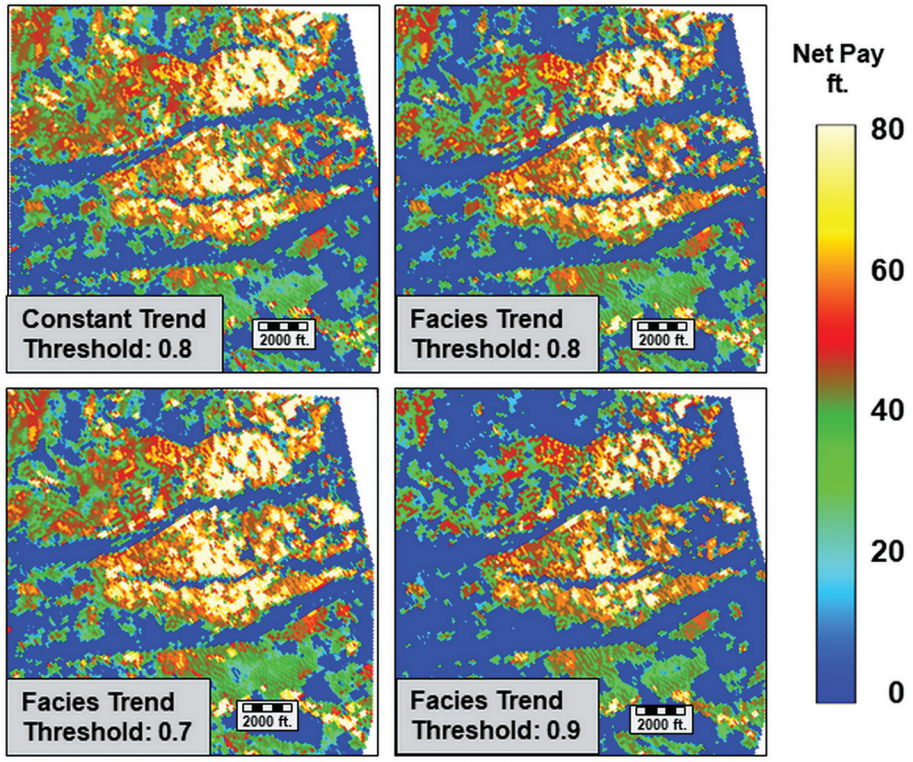

Figure 13. Net pay was computed for the upper green layer from various approaches. The constant trend workflow is shown on the left and the facies-driven workflow is on the right for thresholds of 0.8. The larger net pay in the constant method is due to the presence of more false positives. The bottom images compare the facies-driven method for thresholds of 0.7 and 0.9, where there is less but more reliable net pay. Clinoform development is best evident in the lower left image.

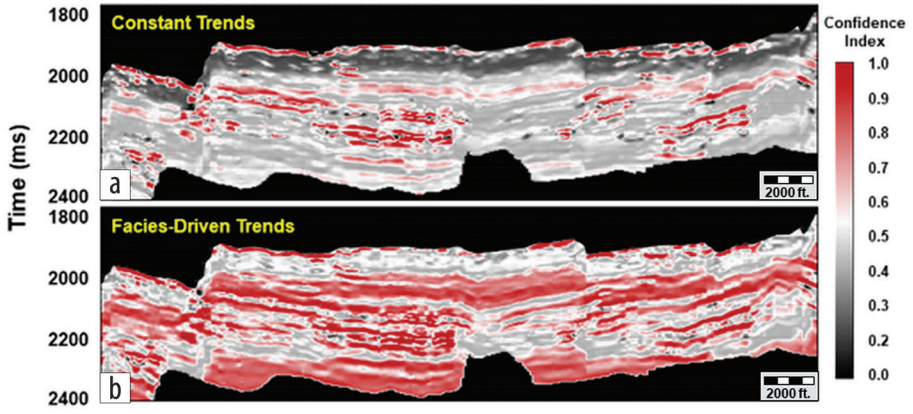

Figure 14. Confidence indices are shown for (a) the constant trend and (b) the facies-driven workflows. The constant trend method exhibits consistently lower values and correspondingly higher uncertainties in facies classifications. The facies-driven method yields estimates with higher probabilities.

Conclusions

We have reviewed the strategies for estimating facies by using Bayesian inference and demonstrated how they can be used to build low-frequency models for optimum seismic inversions without well-log interpolation. The latter, whether simple or employing a more complex function such as kriging, is not considered here because its accuracy between wells cannot be guaranteed. We seek a better approach. We have used a constant structurally compliant elastic trend approach and the idea of a second pass of inversion with low-frequency models computed from facies from the constant trend inversion facies analysis. Neither of these workflows treat the well locations as particularly special, aside from the opportunity to measure the accuracy of our facies measurements. We reasonably expect the same accuracy at interwell locations. We also demonstrated the use of thresholded precision measures and an entropy-based CI to assess the consistency of disparate inversion algorithms and workflows.

An important element in this work was the inclusion of uncertainties in the Bayesian analysis wherever possible. This included accounting for both inversion biases and uncertainties and 3D prior uncertainties. Such accounting generally reduces the probabilities of the most likely facies but is a more reasonable approach when assessing and risking potential drilling locations.

It may be inferred that we discriminate against any low-frequency models that involve well-log interpolation. This is not the case. The optimum interpolation functions are complicated and certainly 3D. They constitute an inversion problem unto themselves. We continue to investigate these methods as a direction for future work. TLE

Acknowledgments

The authors wish to thank Stone Energy for permission to show the seismic data. We also thank the CGG GeoSoftware team for valuable comments and support.

Data and materials availability

Data associated with this research are confidential and cannot be released.

Corresponding author: john.pendrel@cgg.com

References

Debeye, H. W. J., and P. van Riel, 1990, Lp-norm deconvolution: Geophysical Prospecting, **38**, no. 4, 381–403, https://doi.org/10.1111/j.1365-2478.1990.tb01852.x.

Gonzalez, E. F., S. Gesbert, and R. Hofmann, 2016, Adding geologic prior knowledge to Bayesian lithofluid facies estimation from seismic data: Interpretation, **4**, no. 3, SL1–SL8, https://doi.org/10.1190/INT-2015-0220.1.

Guarido, M., 2019, Machine learning strategies to perform facies classification: Presented at CSEG GeoConvention.

Hall, B., 2016, Facies classification using machine learning: The Leading Edge, **35**, no. 10, 906–909, https://doi.org/10.1190/tle35100906.1.

Hall, M., and B. Hall, 2017, Distributive collaborative prediction: Results of the machine learning contest: The Leading Edge, **36**, no. 3, 267–269, https://doi.org/10.1190/tle36030267.1.

Hameed, M., O. Al-Khaled, M. H. A. Razak, and M. Al-Awadhi, 2016, Geostatistical inversion leads to drilling success: A case history from north Kuwait: 86th Annual International Meeting, SEG, Expanded Abstracts, 2886–2890, https://doi.org/10.1190/segam2016-13880273.1.

Hossain, Z., S. Volterrani, and F. Diaz, 2015, Integration of rock physics template to improve Bayes' facies classification: 85th Annual International Meeting, SEG, Expanded Abstracts, 2762–2764, https://doi.org/10.1190/segam2015-5900545.1.

Kemper, M., and J. Gunning, 2014, Joint impedance and facies inversion — Seismic inversion redefined: First Break, **32**, no. 9, 89–95.

Liu, C., D. P. Ghosh, A. M. A. Salim, and W. S. Chow, 2019, A new fluid factor and its application using a deep learning approach: Geophysical Prospecting, **67**, no. 1, 140–149, https://doi.org/10.1111/1365-2478.12712.

Merletti, G. D., and C. Torres-Verdin, 2006, Accurate detection and spatial delineation of thin-sand sedimentary sequences via joint statistical inversion of well logs and 3D pre-stack seismic amplitude data: Presented at Annual Technical Conference and Exhibition, SPE, https://doi.org/10.2118/102444-MS.

Mur, A., and K. Waters, 2018, Play scale seismic characterization: Using basin models as an input to seismic characterization in new and emerging plays: 88th Annual International Meeting, SEG, Expanded Abstracts, 555–559, https://doi.org/10.1190/segam2018-2992809.1.

Nishitsuji, Y., and R. Exley, 2019, Elastic impedance based facies classification using support vector machine and deep learning: Geophysical Prospecting, **67**, no. 4, 1040–1054, https://doi.org/10.1111/1365-2478.12682.

Pendrel, J., and H. J. Schouten, 2019, Entropy QC for Bayesian facies estimations: 89th Annual International Meeting, SEG, Expanded Abstracts, 3151–3155, https://doi.org/10.1190/segam2019-3204859.1.

Pendrel, J., H. Debeye, R. Pedersen-Tatalovic, B. Goodway, J. Dufour, M. Bogaards, and R. Stewart, 2000, Estimation and interpretation of P and S impedance volumes from the simultaneous inversion of P-wave offset data: Presented at CSEG GeoConvention.

Pendrel, J., C. Mangat, and M. Feroci, 2006, Using Bayesian inference to compute facies-fluids probabilities: Presented at CSEG GeoConvention.

Pendrel, J., H. J. Schouten, and R. Bornard, 2016, Accounting for bias and uncertainty in facies estimations from deterministic inversions: 86th Annual International Meeting, SEG, Expanded Abstracts, 2876–2880, https://doi.org/10.1190/segam2016-13528844.1.

Pendrel, J., H. J. Schouten, and R. Bornard, 2017, Bayesian estimation of petrophysical facies and their applications to reservoir characterization: 87th Annual International Meeting, SEG, Expanded Abstracts, 3082–3086, https://doi.org/10.1190/segam2017-17588007.1.

Sams, M., S. Westlake, J. Thorp, and E. Zadeh, 2016, Willem 3D: Reprocessed, inverted, revitalized: The Leading Edge, **35**, no. 1, 22–26, https://doi.org/10.1190/tle35010022.1.

Saussus, D., and M. Sams, 2012, Facies as the key to using seismic inversion for modelling reservoir properties: First Break, **30**, no. 7, 45–52.

Shannon, C. E., 1948, A mathematical theory of communication: The Bell System Technical Journal, **27**, no. 3, 379–423, https://doi.org/10.1002/j.1538-7305.1948.tb01338.x.

Singh, S., S. K. Singh, R. S. Rawat, P. S. Chaudhuri, Harilal, and A. Sood, 2016, Stochastic inversion for thin reservoir delineation: A case study: Presented at 12th International Oil and Gas Conference and Exhibition, PetroTech.

Tao, B., L. Li, W. Wang, F. Mu, and S. Sun, 2016, Establishing the precision sandstone reservoir model using geostatistical inversion: A case study in the South China Sea: 86th Annual International Meeting, SEG, Expanded Abstracts, 3563–3567, https://doi.org/10.1190/segam2016-13712223.1.

Thore, P., 2015, Uncertainty in seismic inversion: What really matters?: The Leading Edge, **34**, no. 9, 1000–1002, https://doi.org/10.1190/tle34091000.1.

Varga, R., R. Lotti, A. Pachos, T. Holden, I. Marini, E. Spadafora, and J. Pendrel, 2012, Seismic inversion in the Barnett Shale successfully pinpoints sweet spots to optimize well-bore placement and reduce drilling risks: 82nd Annual International Meeting, SEG, Expanded Abstracts, https://doi.org/10.1190/segam2012-1266.1.

Yenwongfai, H., N. H. Mondol, I. Lecomte, J. I. Faleide, and J. Leutcher, 2019, Integrating facies-based Bayesian inversion and supervised machine learning for petro-facies characterization in the Snadd Formation of the Goliat Field, south-western Barents Sea: Geophysical Prospecting, **67**, no. 4, 1020–1039, https://doi.org/10.1111/1365-2478.12654.